



Figures and figure supplements

Synaptic mechanisms underlying modulation of locomotor-related motoneuron output by premotor cholinergic interneurons

Filipe Nascimento *et al*

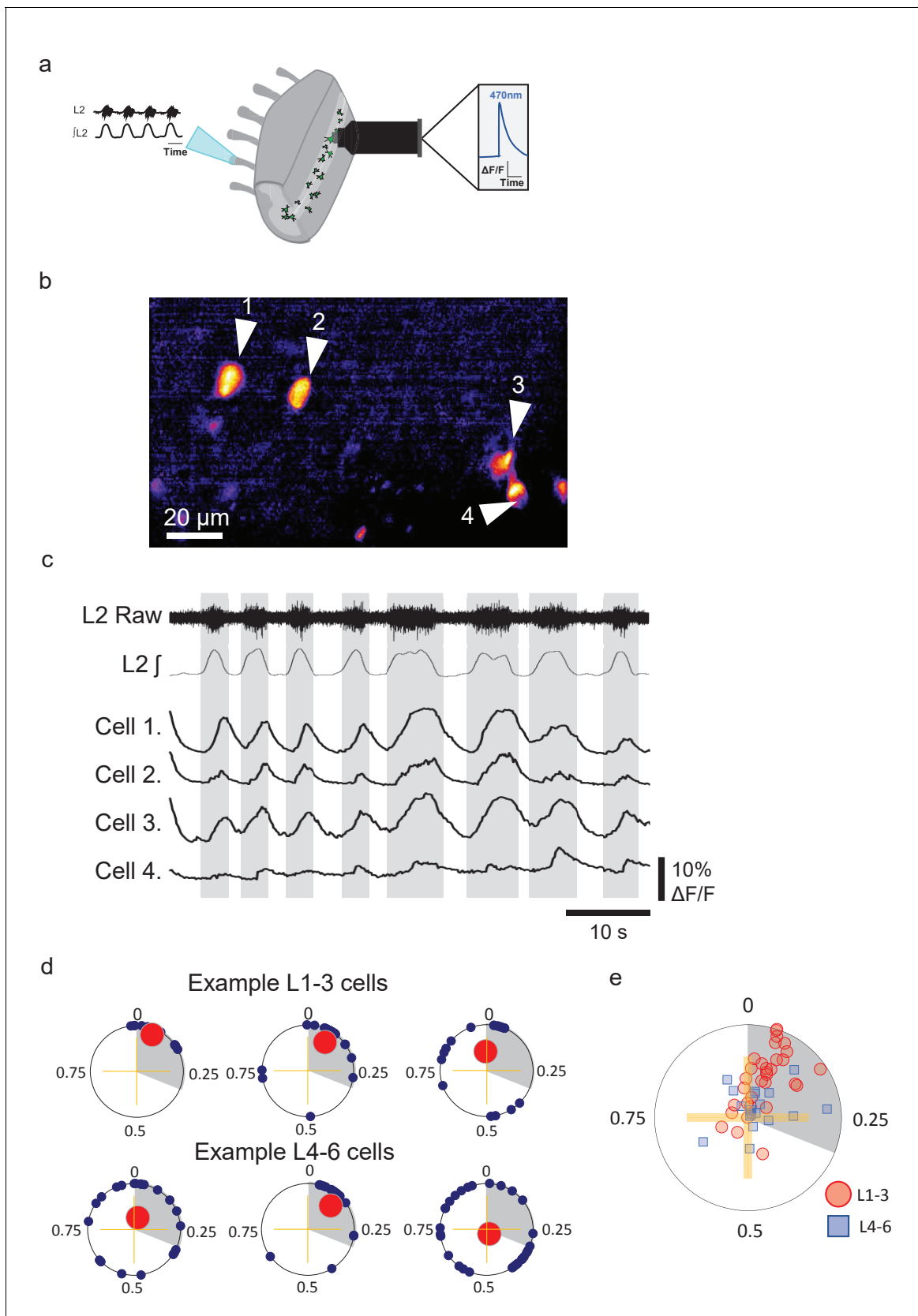


Figure 1. Groups of lumbar *Pitx2*⁺ interneurons are rhythmically active during fictive locomotion. **(a)** Illustration of ventral root recordings and Ca^{2+} imaging from *Pitx2*⁺ interneurons (green) in hemisected spinal cords from *Pitx2::Cre;GCAMP6* mice. **(b)** *Pitx2*⁺ interneurons visualized in the L1-3 upper Figure 1 continued on next page

Figure 1 continued

lumbar regions in a neonatal hemisected spinal cord from a *Pitx2::Cre;GCAMP6* mouse. (c) Ventral root output and examples of Ca^{2+} imaging traces from the four neurons marked in (b). (d) Phase plots depicting relationships between Ca^{2+} transients in interneurons and ventral root output for three neurons in L1-3 (top) and three neurons in L4-6 (bottom). Blue points represent the phasing of individual Ca^{2+} transients within a locomotor cycle, red points represent the mean direction and strength of the phasing for each neuron, and grey shading indicates the average duration of upper lumbar-related bursts. (e) Summary graph of mean direction and strength of phasing for all interneurons analyzed (L1-3, $n=31$; and L4-6, $n=19$).

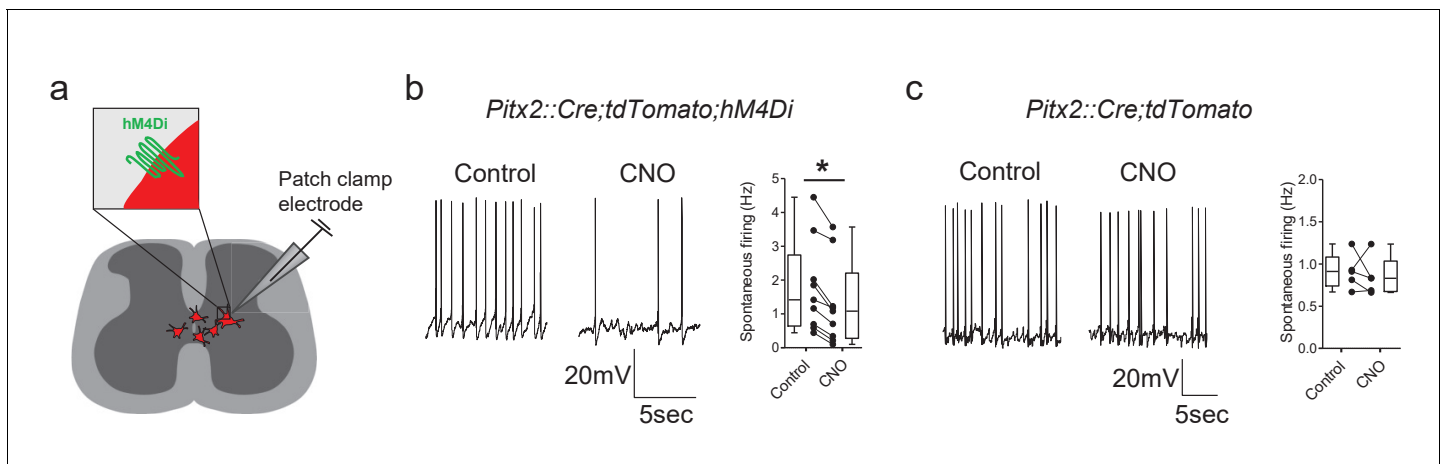


Figure 2. The activity of Pitx2⁺ interneurons can be decreased using DREADDs. (a) Schematic representation of a spinal cord slice containing Pitx2⁺ interneurons (red) targeted for single-cell recordings. (b and c) Spontaneous firing of Pitx2⁺ interneurons from *Pitx2::Cre;tdTomato;hM4Di* (b) and *Pitx2::Cre;tdTomato* (c) mice in control conditions and in the presence of CNO (1 μ M); along with firing frequency data pooled for all recordings (b, n = 9; c, n = 5). *p<0.05.

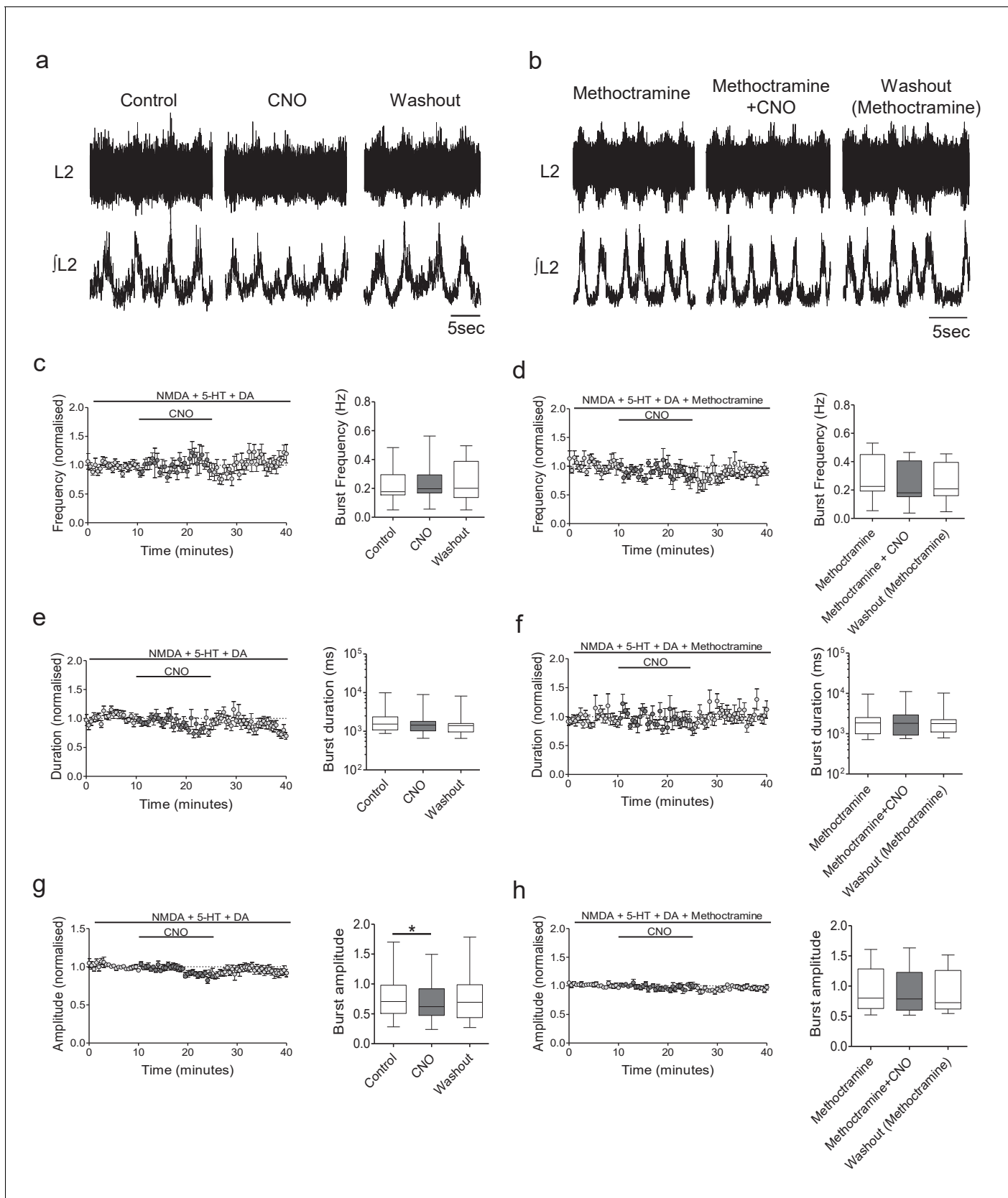


Figure 3. Inhibition of Pitx2^+ interneurons during fictive locomotion decreases burst amplitude in an M2 receptor-dependent manner. (a and b) Raw (top) and integrated/rectified (bottom) traces illustrating the effects of (a) CNO (1 μM) and (b) CNO plus methoctramine (10 μM) on drug-induced

Figure 3 continued on next page

Figure 3 continued

locomotor output recorded from spinal cords of Pitx2::Cre;hM4Di mice. (c – h) Time course plots and box-plots of pooled data showing the effects of CNO alone or CNO plus methoctramine on locomotor burst frequency (**b,c**), duration (**d,e**) and amplitude (**g,h**). * $p < 0.05$.

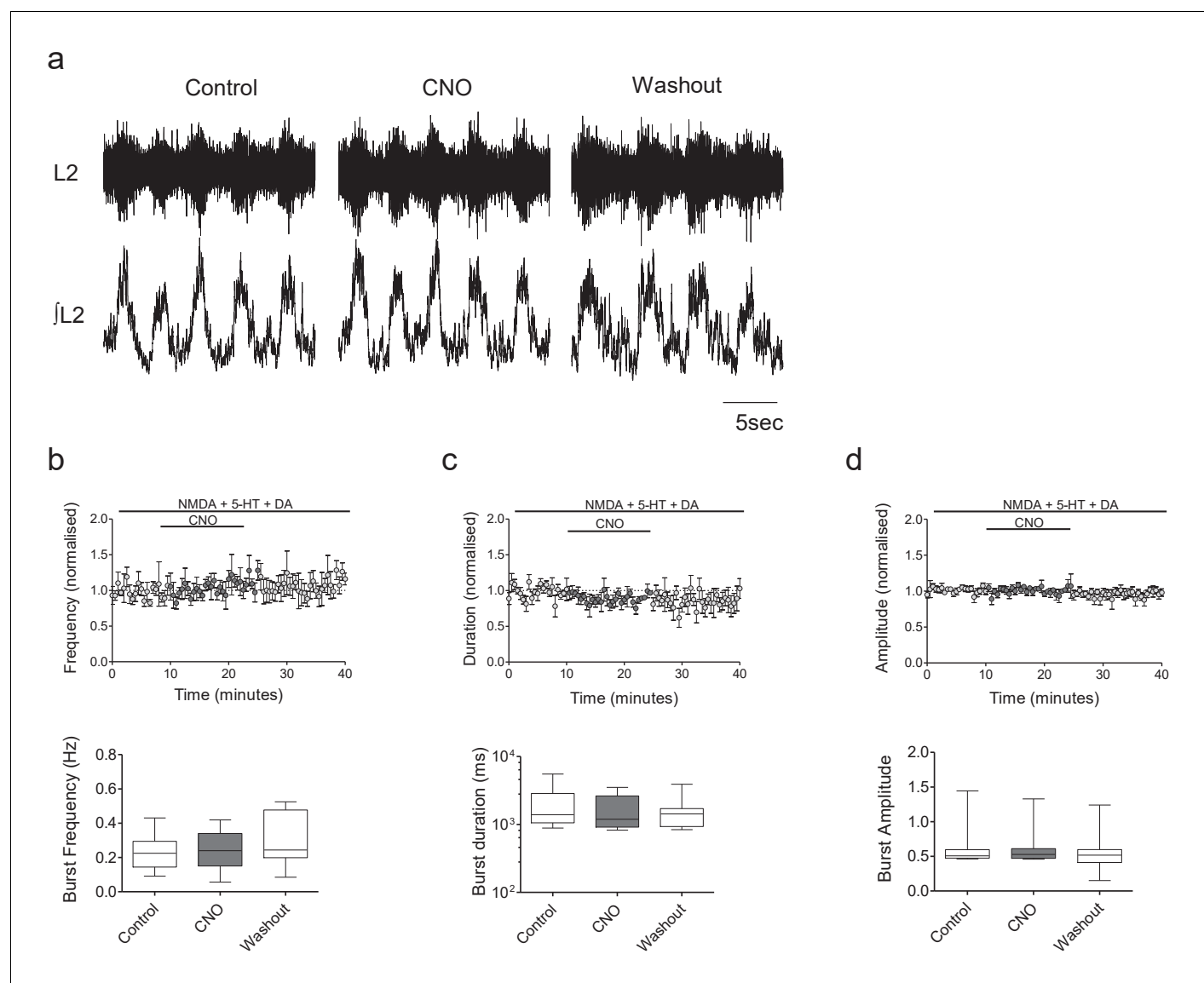


Figure 3—figure supplement 1. CNO has no effect on ventral root output in control *hM4Di* mice. (a) Raw (top) and integrated/rectified (bottom) traces showing locomotor-related ventral root bursts recorded from the spinal cord of a *hM4Di* mouse in control, CNO and wash conditions. (b–d) Average time course plots (top) and mean pooled data (bottom) showing no significant effect of CNO (1 μ M) on the frequency (b), duration (c) or amplitude (d) of drug-induced locomotor output recorded from the spinal cords of *hM4Di* mice (n = 8).

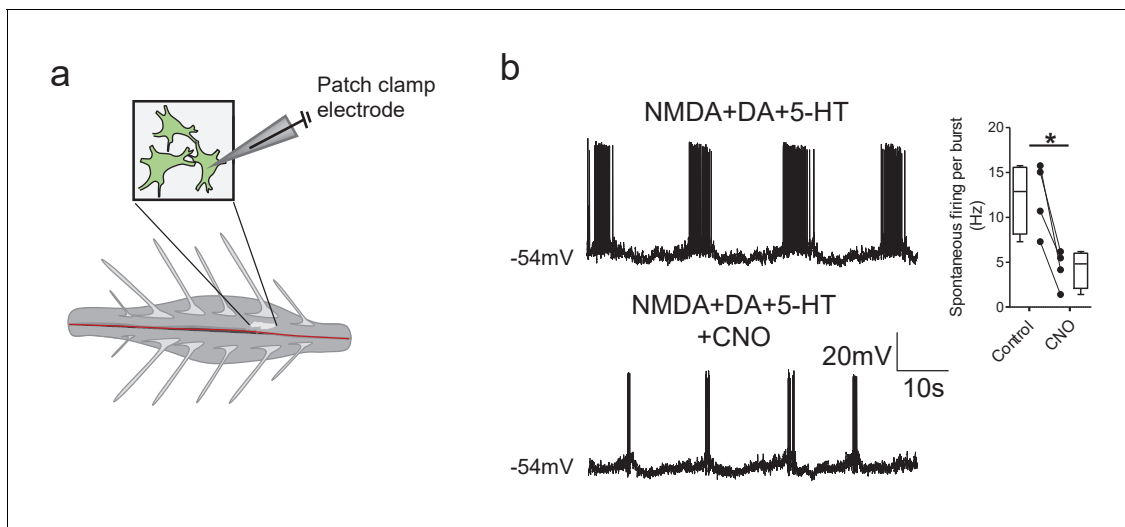


Figure 4. DREADD-mediated inhibition of Pitx2⁺ interneurons decreases motoneuron firing rates during fictive locomotion. (a) Schematic depicting the intact spinal cord preparation used for patch clamp recordings of lumbar motoneurons (green) during fictive locomotion. (b) Spontaneous firing recorded from a motoneuron during pharmacologically induced fictive locomotion in control conditions and after the addition of CNO; along with firing frequency data pooled for all recordings (n = 4); *p<0.05.

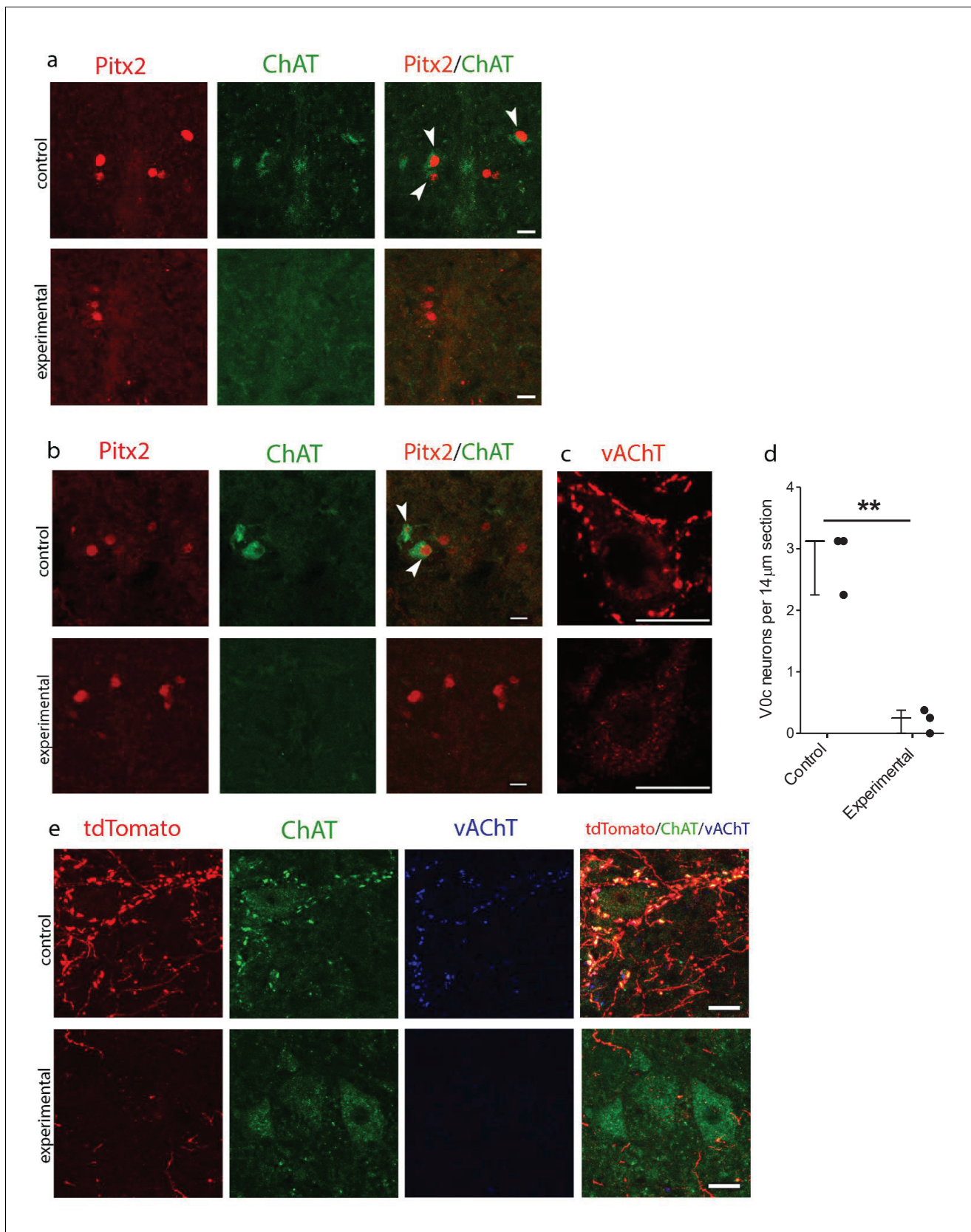


Figure 5. Genetic ablation of cholinergic $Pitx2^+$ interneurons (V0c) eliminates C-boutons around motoneuron somata. (a) Immunofluorescence in spinal cord sections of P2 wt (control) and $Pitx2::Cre;vAChT-stop-DTA$ (experimental) mice using antibodies against Pitx2 (red) and Choline Acetyl Transferase

Figure 5 continued on next page

Figure 5 continued

(ChAT, green). (b) Immunofluorescence in spinal cord sections of P7 upper lumbar levels from wt (control) and *Pitx2::Cre;;vAChT-stop-DTA* (experimental) mice using antibodies against Pitx2 (red) and ChAT (green). White arrows in (a) and (b) point to double positive neurons. Neurons that are positive for cholinergic markers only but not positive for Pitx2 are preganglionics, typically present in the intermediate zone in these levels (a, b). (c) Immunofluorescence of motoneurons and their C-bouton terminals in upper lumbar spinal cord sections using an antibody against vAChT. (d) Average number of V0c neurons per 14 μm section in control and experimental P7 mice. (e) Immunofluorescence of motoneurons and their C-bouton terminals in upper lumbar spinal cord sections of P25 *Pitx2::Cre;tdTomato* (control) and *Pitx2::Cre;tdTomato;vAChT-stop-DTA* (experimental) mice using antibodies against tdTomato (red), ChAT (green) and vAChT (blue); Photos acquired with confocal microscopy using (a, b) 20x lens and (c, e) 40x lens. Sections thickness was 14 μm and scale bar is 20 μm ; n = 3 mice for each condition; **p<0.01.

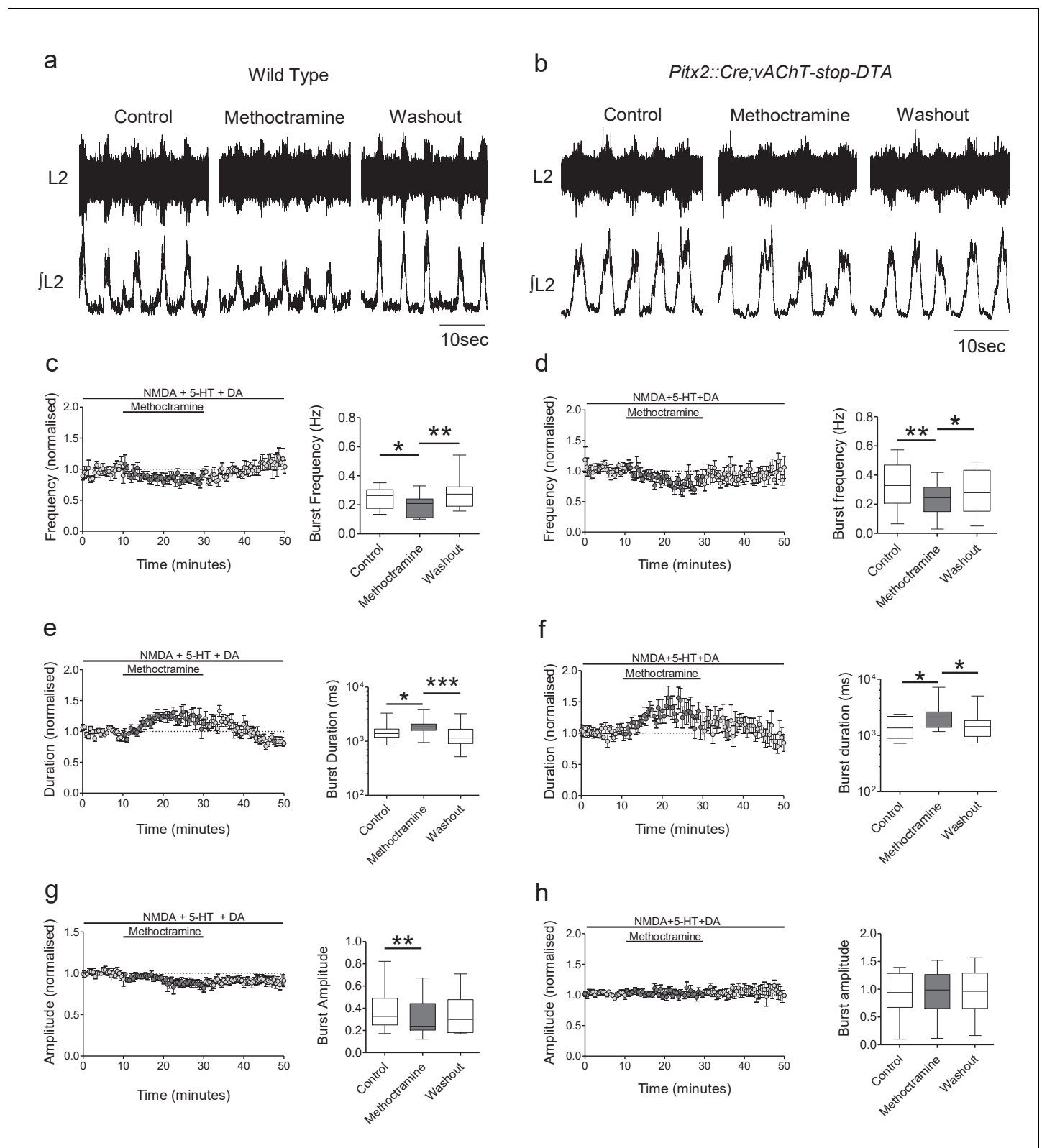


Figure 6. Genetic ablation of cholinergic *Pitx2*⁺ interneurons (V0c) removes M2 receptor-dependent modulation of locomotor burst amplitude. (a, b) Raw (top) and integrated/rectified (bottom) traces with averaged time course plots and mean pooled data illustrating the effects of methoctramine (10 μ M) on Wild Type (n = 12) and *Pitx2::Cre;vAChT-stop-DTA* (n = 10) mice lumbar ventral root burst frequency (c, d), duration (e, f) and amplitude (g, h); *p<0.05, **p<0.01, ***p<0.001.

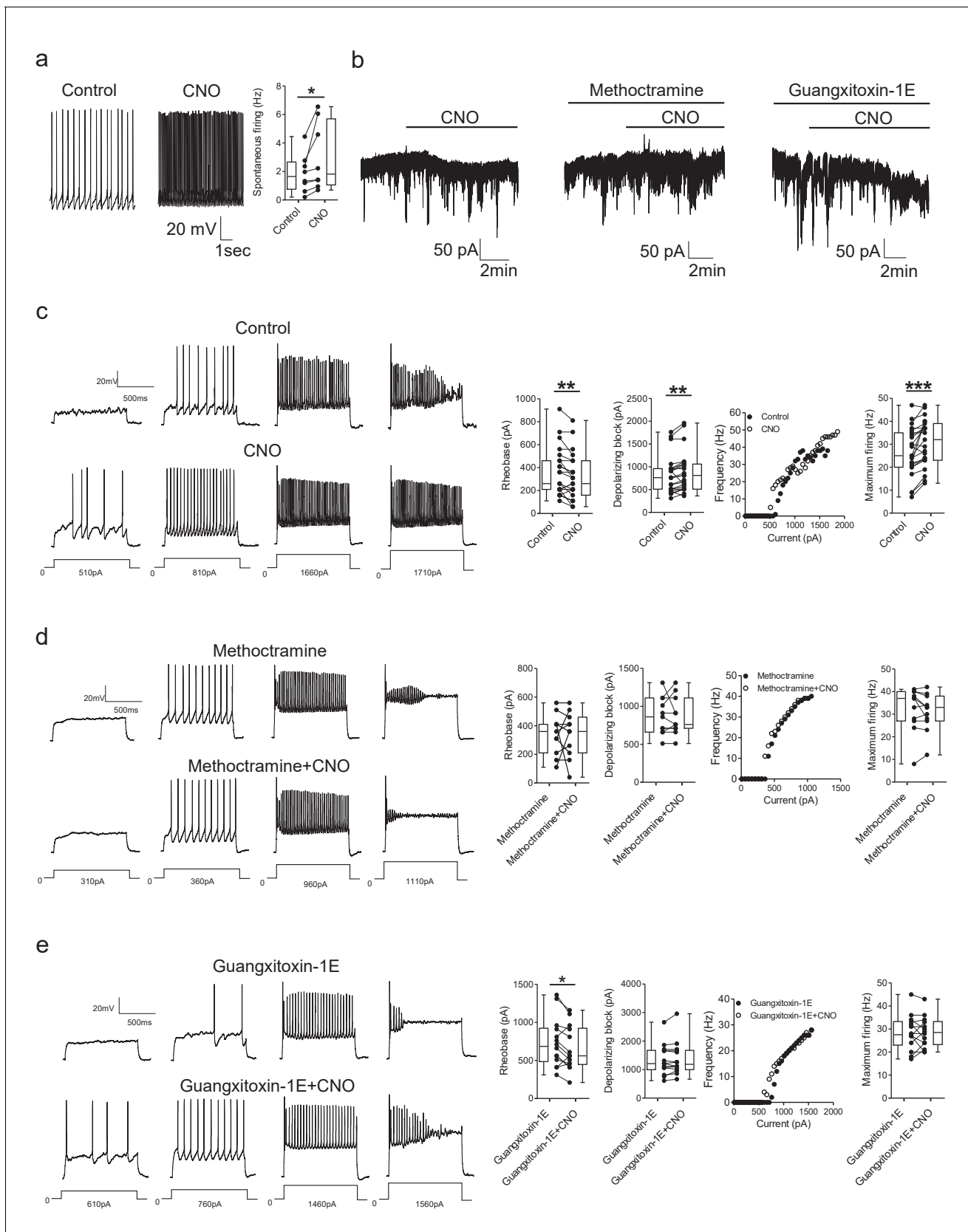


Figure 7. DREADD-based activation of Pitx2^+ interneurons increases motoneuron firing via M2 receptors and Kv2.1 channels. (a) Spontaneous firing of a Pitx2^+ interneuron from a $\text{Pitx2}::\text{Cre};\text{tdTomato};\text{hM3Dq}$ mouse in control conditions and during the application of CNO; along with firing frequency

Figure 7 continued on next page

Figure 7 continued

data pooled for all recordings ($n = 8$). **(b)** Representative traces illustrating changes in holding current ($V_{\text{hold}} = -60$ mV) during recordings of motoneurons in the presence of CNO alone (left) or co-applied with methoctramine ($10 \mu\text{M}$, middle) or guangxitoxin-1E (50 nM, right). **(c)** Motoneuron firing in response to current steps in control conditions and in the presence of CNO (left) with pooled data plotted to show changes in rheobase, depolarizing block, current-frequency relationships and maximum firing (right) ($n = 23$). **(d, e)** Examples of motoneuron firing and pooled data depicting firing parameters in the presence of methoctramine and methoctramine co-applied with CNO (**d**; $n = 11$) or Guangxitoxin-1E and CNO co-applied with Guangxitoxin-1E (**e**; $n = 14$). * $p > 0.05$, ** $p < 0.01$, *** $p < 0.001$.

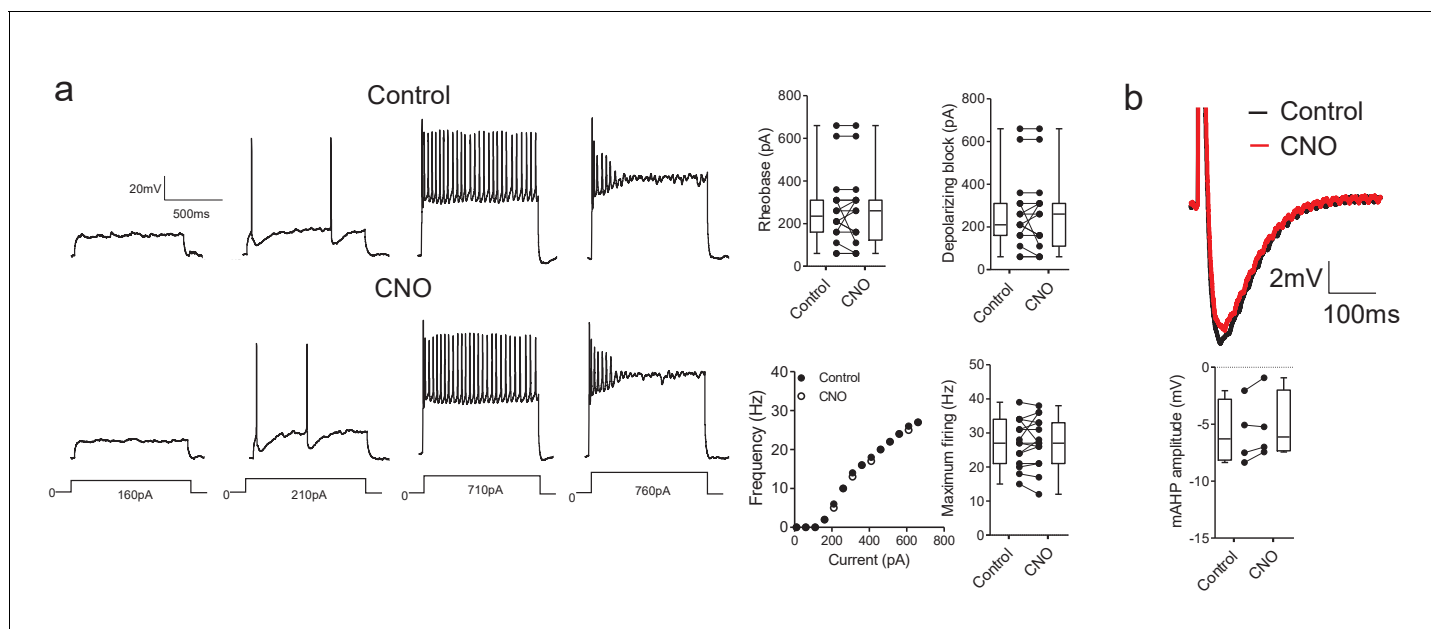


Figure 7—figure supplement 1. CNO has no effect on motoneuron properties in *hM3Dq* mice. (a) CNO does not effect motoneuron firing parameters (rheobase, depolarizing block, current-frequency relationships or maximum firing rates, $n = 15$) and (b) mAHP amplitude ($n = 4$) in mice that do not express DREADD receptors. Input resistance also did not change in the presence of CNO (control: $77 \pm 12 \text{ M}\Omega$, CNO: $78 \pm 12 \text{ M}\Omega$, $t(9)=0.499$, Paired t-test, $p=0.6295$).

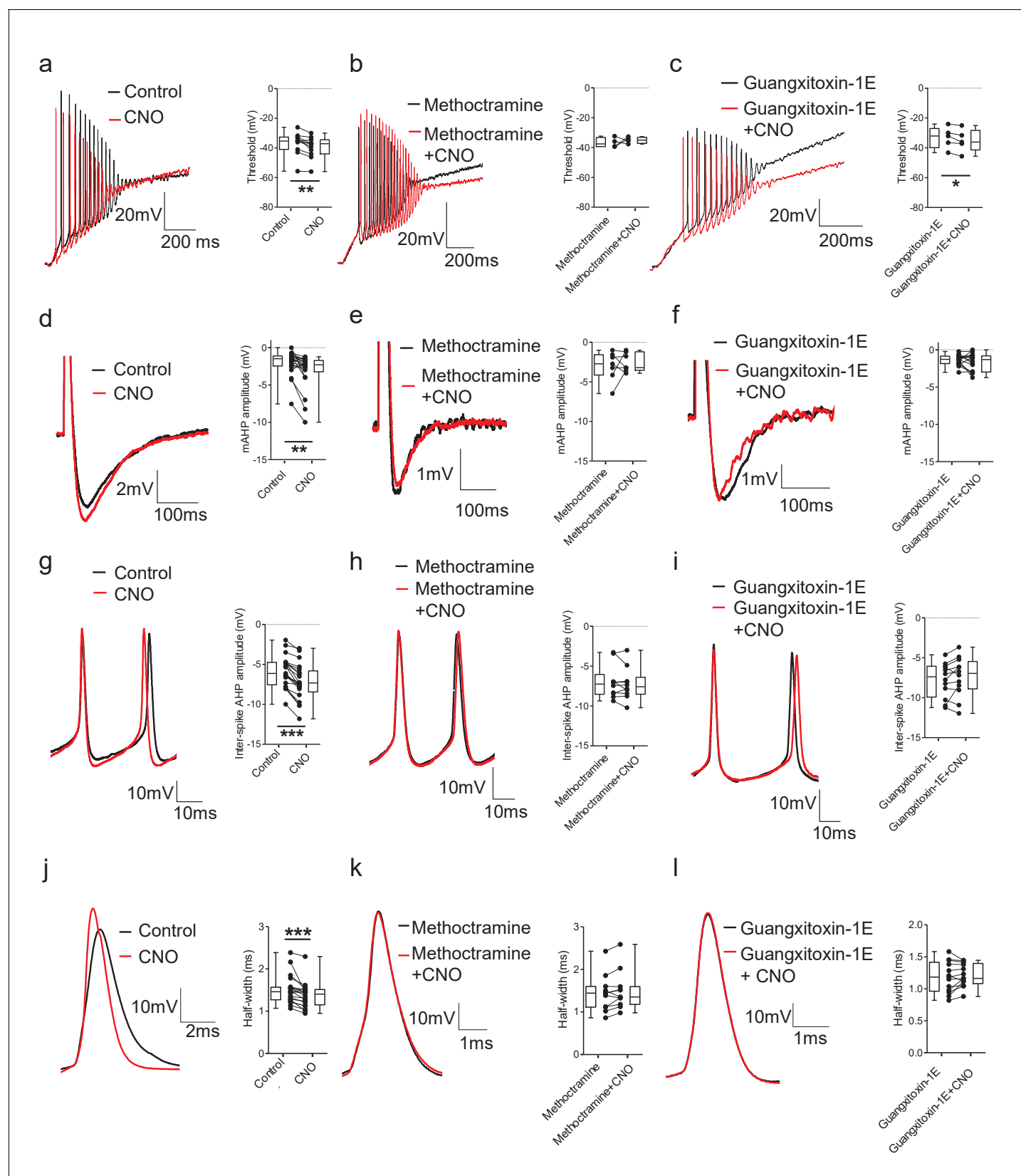


Figure 8. DREADD-based activation of $Pitx2^+$ interneurons influences action potential parameters in motoneurons. (a–c) Motoneuron firing in response to depolarizing current ramps (1 s duration) in whole spinal cord preparations from *Pitx2::Cre;hM3Dq* mice demonstrating action potential threshold Figure 8 continued on next page

Figure 8 continued

following activation of Pitx2⁺ interneurons with CNO alone (a; 1 μ M, a; n = 12), and CNO co-applied with either methoctramine (10 μ M) (b; n = 4) or guangxitoxin-1E (50 nM) (c; n = 5). (d–f) Truncated single action potentials illustrating the amplitude of the mAHP following application of CNO alone (d; n = 22), and CNO co-applied with either methoctramine (e; n = 7) or guangxitoxin-1E (f; n = 11). (g–i) Successive action potentials recorded during repetitive firing showing inter-spike AHP amplitude following application of CNO alone (g; n = 21), and CNO co-applied with either methoctramine (h; n = 10) or guangxitoxin-1E (i; n = 12). (j–l) Recordings of single action potentials illustrating action potential half-width following application of CNO alone (j; n = 20), and CNO in the presence of either methoctramine (k; n = 11) or guangxitoxin-1E (l; n = 13). *p<0.05, **p<0.01, ***p<0.001.

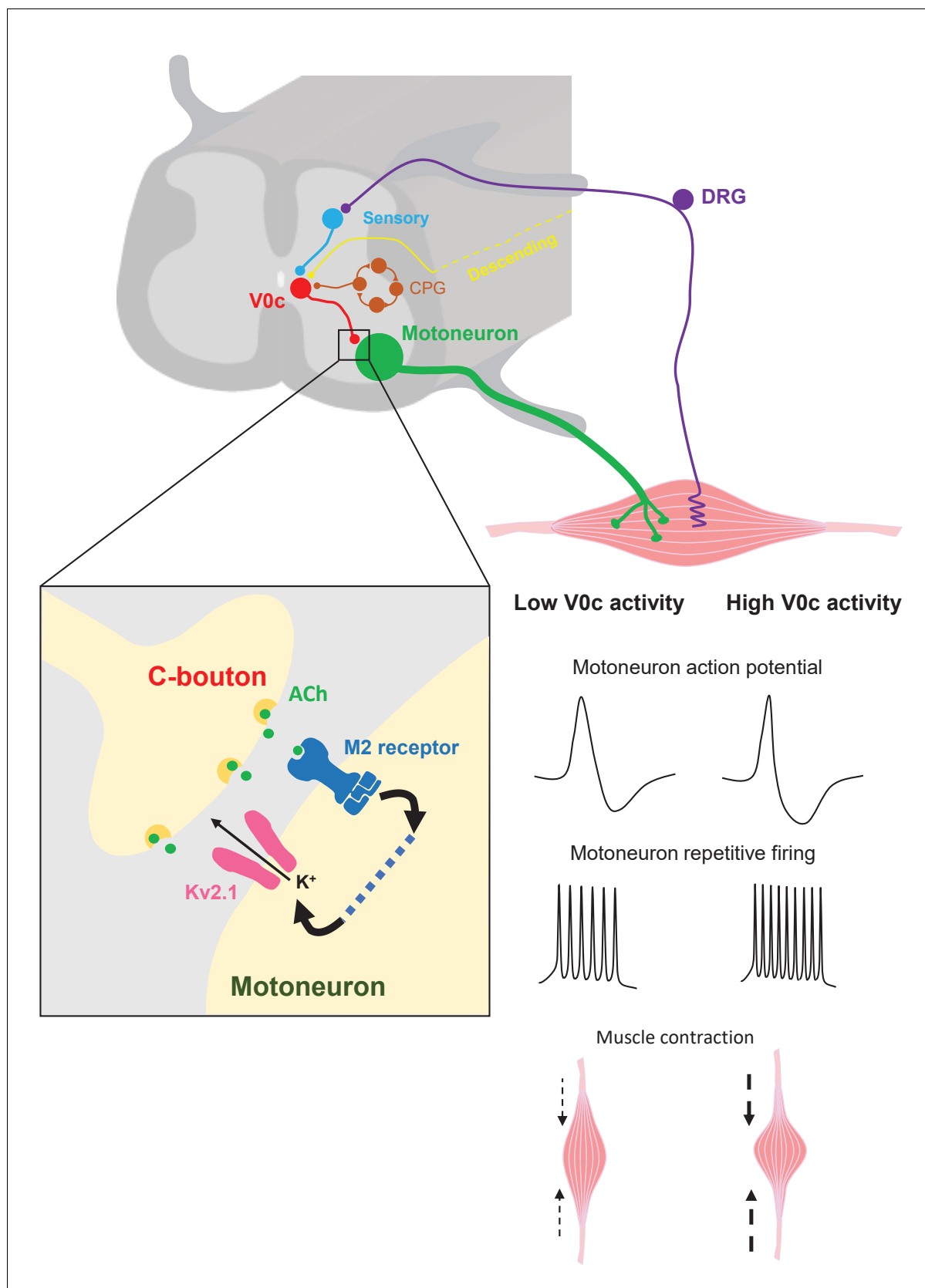


Figure 9. Mechanisms of V0c interneuron-mediated modulation of motor output. V0c interneurons (red) form C-bouton synapses on motoneurons (green) and are known to receive disynaptic inputs from sensory afferents (blue) as well as input from local CPG neurons (orange) and higher brain. Figure 9 continued on next page

Figure 9 continued

regions (yellow) (**Zagoraïou et al., 2009**). Activation of V0c interneurons will lead to release of acetylcholine at C-bouton synapses, activation of postsynaptic M2 muscarinic receptors on motoneurons, and subsequent facilitatory regulation of Kv2.1 channels via as yet uncharacterized signaling pathways (dotted blue line). This modulation leads to an increase in inter-spike AHP and a decrease in action potential duration, allowing for increased and sustained motoneuron firing output, which will translate into more intense muscle contraction (DRG = dorsal root ganglion).